ANNALS OF GEOPHYSICS, 57, 3, 2014, SS0323; doi:10.4401/ag-6382

Special section: Geophysical monitorings at the Earth's polar regions

Observations of surface radiation and stratospheric processes at Thule Air Base, Greenland, during the IPY

Giovanni Muscari[1,*], Claudia Di Biagio[2,3,7], Alcide di Sarra[2], Marco Cacciani[4], Svend Erik Ascanius[5], Pietro Paolo Bertagnolio[1,3], Claudio Cesaroni[1,4], Robert L. de Zafra[6], Paul Eriksen[5], Giorgio Fiocco[4], Irene Fiorucci[1], Daniele Fuà[4]

[1] *Istituto Nazionale di Geofisica e Vulcanologia, Rome, Italy*

[2] *ENEA, Laboratory for Earth Observations and Analyses, Santa Maria di Galeria, Italy*

[3] *Università di Siena, Dipartimento Scienze fisiche, della Terra e dell'ambiente, Siena, Italy*

[4] *La Sapienza - Università di Roma, Dipartimento di Fisica, Rome, Italy*

[5] *Danish Meteorological Institute, Copenhagen, Denmark*

[6] *State University of New York, Department of Physics and Astronomy, Stony Brook, NY, USA*

[7] *Now at LISA, UMR CNRS 7583, Universités Paris Est Créteil et Paris Diderot, Institut P.S. Laplace, Créteil, France*

Article history
Received June 30, 2013; accepted October 25, 2013.
Subject classification:
Polar atmosphere, NDACC, Radiative budget, Stratospheric ozone.

ABSTRACT

Ground-based measurements of atmospheric parameters have been carried out for more than 20 years at the Network for the Detection of Atmospheric Composition Change (NDACC) station at Thule Air Base (76.5 °N, 68.8 °W), on the north-western coast of Greenland. Various instruments dedicated to the study of the lower and middle polar atmosphere are installed at Thule in the framework of a long standing collaboration among Danish, Italian, and US research institutes and universities. This effort aims at monitoring the composition, structure and dynamics of the polar stratosphere, and at studying the Arctic energy budget and the role played by different factors, such as aerosols, water vapour, and surface albedo. During the International Polar Year (IPY), in winter 2008-2009, an intensive measurement campaign was conducted at Thule within the framework of the IPY project "Ozone layer and UV radiation in a changing climate evaluated during IPY" (ORACLE-O3) which sought to improve our understanding of the complex mechanisms that lead to the Arctic stratospheric O_3 depletion. The campaign involved a lidar system, measuring aerosol backscatter and depolarization ratios up to 35 km and atmospheric temperature profiles from 25 to 70 km altitude, a ground-based millimeter-wave spectrometer (GBMS) used to derive stratospheric mixing ratio profiles of different chemical species involved in the stratospheric ozone depletion cycle, and then ground-based radiometers and a Cimel sunphotometer to study the Arctic radiative budget at the surface. The observations show that the surface radiation budget is mainly regulated by the longwave component throughout most of the year. Clouds have a significant impact contributing to enhance the role of longwave radiation. Besides clouds, water vapour seasonal changes produce the largest modification in the shortwave component at the surface, followed by changes in surface albedo and in aerosol amounts. For what concerns the middle atmosphere, during the first part of winter 2008-2009 the cold polar vortex allowed for the formation of polar stratospheric clouds (PSCs) which were observed above Thule by means of the lidar. This period was also characterized by GBMS measurements of low values of O_3 due to the catalytic reactions prompted by the PSCs. In mid-January, as the most intense Sudden Stratospheric Warming event ever observed in the Arctic occurred, GBMS and lidar measurements of O_3, N_2O, CO and temperature described its evolution as it propagated from the upper atmosphere to the lower stratosphere.

1. Introduction

In 1988, the atmospheric physics group of the "Sapienza" University of Rome (UR) and the Danish Meteorological Institute (DMI) started planning the installation of a lidar for the investigation of the Arctic stratosphere at Thule Air Base (TAB; 76.5°N, 68.8°W), Greenland, where the DMI had started setting up a scientific station dedicated to the Arctic climate. Thule Air Base is a military base of the United States Air Force (USAF), founded in 1951 and located on the north-western coast of Greenland, bordering Baffin Bay. The main base is located in a valley facing westward to the sea and enclosed between South Mountain and North Mountain, which each have an elevation of about 250 m above sea level. Thule is equipped with a dock, op-

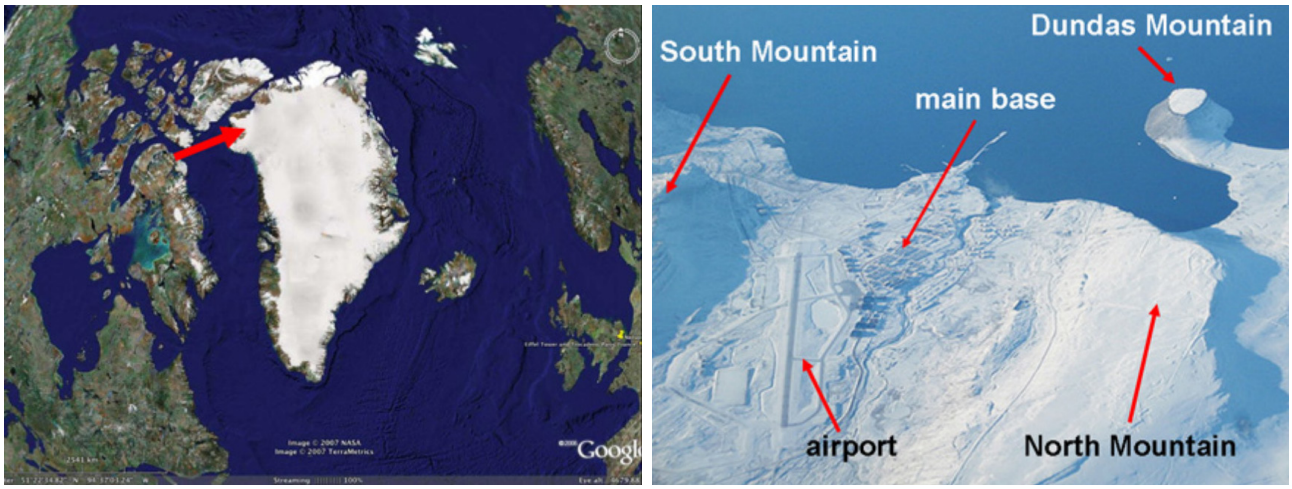

Figure 1. Left: geographical map of Greenland, with the position of Thule Air Base indicated with a red arrow. Right: aerial view of Thule.

erational only in summertime, and an airport which is operational all year round. An aerial view of the base is shown in Figure 1.

The Rayleigh lidar was installed at Thule during fall 1990 (see Figure 2). The main scientific objective was to improve knowledge of the stratospheric ozone depletion phenomenon that was observed to be very intense over Antarctica and anticipated to become important also over the Arctic. In particular, the collaboration set out to detect stratospheric aerosol/cloud particles by means of the UR ground-based lidar system which added to the DMI capability to measure stratospheric ozone profiles inside the polar vortex by ozonesondes and total ozone with a SAOZ spectrometer. The installation of the lidar took approximately 3 weeks of intense field work and involved 4 researchers from UR and DMI as well as several technicians and carpenters which set up electrical switches for the laser and built the roof hatch for the lidar's telescope. Initially, the lidar had only two receiving channels, used to observed the backscattered parallel- and cross-polarized signals from the stratosphere, which were digitalized and then saved by means of a 286 Olivetti PC.

During the following ~20 years, also in the context of large European measurement programs (i.e., the European Arctic Stratospheric Ozone Experiment, EASOE; the Second European Stratospheric Arctic Ozone Experiment, SESAME, and others), the DMI expanded its activities at Thule, additional instruments were installed, and the collaboration with the University of Rome was extended to other Italian (Istituto Nazionale di Geofisica e Vulcanologia - INGV, and ENEA) and US (National Center for Atmospheric Research - NCAR, and Stony Brook University) research institutes. In particular, in January 2009, the participation of DMI, UR, ENEA, and INGV to International Polar Year (IPY) activities were partly supported by the US National Science Foundation, the Italian Antarctic Programme (PNRA) and Ministry for University and Research, and allowed the installation of additional instruments. The ground-based millimeter-wave spectrometer (GBMS) (Figure 3) was brought back to Thule (after having conducted 2 successful campaigns measuring the stratospheric trace gases N_2O, O_3 and ClO in 1992 in and 1993, and again in 2001-2002 and 2002-2003) [e.g., Muscari et al. 2007] to contribute to the knowledge of stratospheric chemistry with measurements of stratospheric O_3 and HNO_3. The measurements during the IPY were conducted within the IPY project "Ozone layer and UV radiation in a changing climate evaluated during IPY" (ORACLE-O3) aimed at improving our understanding

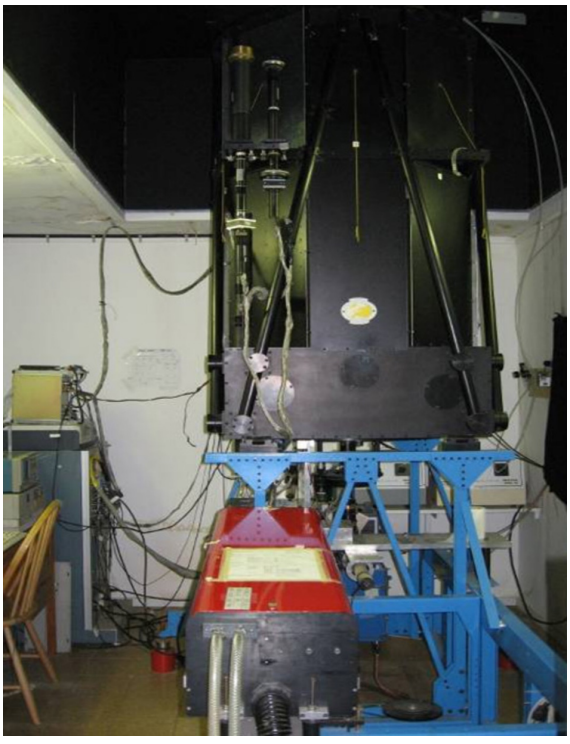

Figure 2. The lidar installed at Thule.

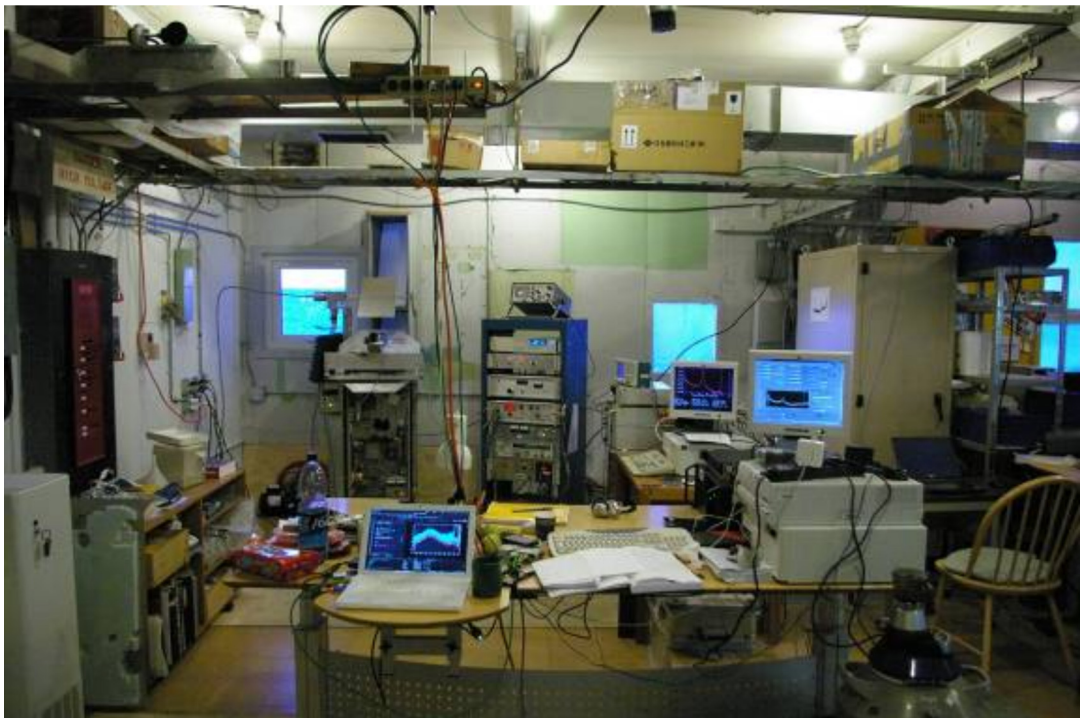

Figure 3. The GBMS installed at Thule, with the receiver facing the mm-wave window.

of the complex mechanisms that lead to the Arctic stratospheric O_3 depletion, therefore including the physico-chemical processes that form the polar stratospheric clouds and the heterogeneous reactions that take place on the surface of PSC particles.

At the South Mountain laboratory (building #1985, at a 20-minute drive from main base), the NCAR and the DMI installed a Fourier Transform InfraRed spectrometer (FTIR) and a UV spectrometer in the late 90s. These instruments, together with the lidar and the GBMS, actively contribute to the Network for Detection of Atmospheric Composition Change (NDACC; http://www.ndsc.ncep.noaa.gov/), which is a global network of measurements stations for the monitoring of the atmospheric composition and climate.

In addition to observing processes that affect the stratospheric ozone, the NDACC station at Thule is dedicated to study the parameters that play a key role in regulating the Arctic climate and its influence on the global scale. In fact, the Arctic region is among the most sensitive to climate change, due to peculiar conditions and some specific phenomena linked to the evolution of sea ice, its influence on the radiation budget and the involved feedback mechanisms [McGuire et al. 2006, Serreze and Francis 2006]. A growing attention has been dedicated in recent years to the study of the role of atmospheric aerosols, and in particular to the phenomenon of the Arctic haze [Quinn et al. 2007], which may affect the Arctic radiative balance. In order to investigate these phenomena, in 2002 the DMI installed a radiometer on the roof of building #1985 for measuring the ground-level shortwave irradiance (see Figure 4). In 2007 a Cimel sunphotometer (part of the AErosol RObotic NETwork, or AERONET; http://aeronet.gsfc.nasa.gov/) for the measurement of aerosol physical properties and column water vapour was added

Figure 4. The TSP-700 and the PIR 33499 installed on the roof of buiding #1985.

Figure 5. The Cimel installed on the roof of building #1985.

to it (see Figure 5), and in 2009 the lidar was upgraded through the addition of two new receiving telescopes for the investigation of the troposphere and surface boundary layer (see Figure 6).

In this study the surface radiative budget and the evolution of the stratospheric structure and composition at Thule during the IPY will be described using data collected with ground-based radiometers, the Cimel sunphotometer, the GBMS, and the lidar.

2. Instruments description

As previously discussed, different instruments are installed at Thule for measuring atmospheric composition and structure, the radiation budget at the surface, and the aerosol physical properties. The following sections contain a description of the instruments whose observations are used for these studies.

2.1. The Rayleigh LIDAR

The LIDAR (LIght Detection And Ranging) is an active remote sensing instrument based on the same principle of operation of a radar but with a radiation source, a laser, emitting in the UV, visible, or near IR spectral range. Molecules and particles present in the atmosphere interact with the laser emitted light pulses through processes of scattering and absorption, and return an echo signal which is measured by the lidar receiving system.

A picture and the scheme of the lidar installed at TAB are shown in Figures 2 and 6. The emitting unit is a two-stage Nd:YAG laser with a second harmonic generator producing linearly polarized pulses at 532 nm, with a repetition rate of 10 Hz. A prism is used to direct the laser beam vertically into the atmosphere. The receiver includes a 800 mm diameter Cassegrain telescope for the upper troposphere and middle atmosphere, and two 64 mm diameter telescopes for the troposphere. The signal collected by each of the three telescopes is focused and filtered to select only elastic backscattered signals. Each channel is equipped with a photomultiplier (PMT). A chopper is used in combination with the 800 mm telescope to cut off the signal from the lowest atmospheric levels to prevent the saturation of the photomultiplier tubes.

The acquisition system is composed by electronic units that include both analog and photon counting acquisition channels. The analog signal detection is used for the low altitude channels, while the photon counting is preferred for the high altitude ones. The total signal and the parallel polarized component (with respect to the polarization of the emitted radiation) are separately acquired for the low channels, while the parallel and the cross polarized components of the backscattered signal are acquired for the high channels.

The lidar has been operational during several years since its installation in 1990, particularly during winter seasons [i.e., di Sarra et al. 1992, Di Girolamo et al. 1994, Larsen et al. 1994, di Sarra et al. 1995, Marenco et al. 1997, di Sarra et al. 2002, Muscari et al. 2007, Di Biagio et al. 2010]. In 1993 the capability to perform daytime measurements of clouds and particles in the upper troposphere and lower stratosphere was added [di Sarra et al. 1998]. This improvement allowed to follow the evolution of stratospheric particles in the lower stratosphere after the 1991 eruption of volcano Pinatubo. At the same time, nighttime measurements of the middle atmosphere temperature profile were started [Marenco et al. 1997, Muscari et al. 2007].

During the IPY the lidar operational at TAB derived measurements of:

(1) aerosol backscatter and depolarization ratio profiles from 0.2 to 25-30 km altitude with a vertical resolution of 30 m and a temporal resolution of few minutes. Aerosol measurements were made both in daytime and nighttime;

(2) density and temperature profiles from 25-35 to 70 km with a vertical resolution of about 4.5 km. To increase the signal-to-noise ratio the signal was integrated for 1-5 hours (the integration time mainly depends on the weather conditions and on the possibility to make measurements). Density and temperature measurements were possible only during nighttime.

2.2. Ground-based millimeter-wave spectrometer (GBMS)

The ground-based millimeter-wave spectrometer (GBMS) [de Zafra 1995] measures rotational emission spectra of atmospheric chemical species such as O_3,

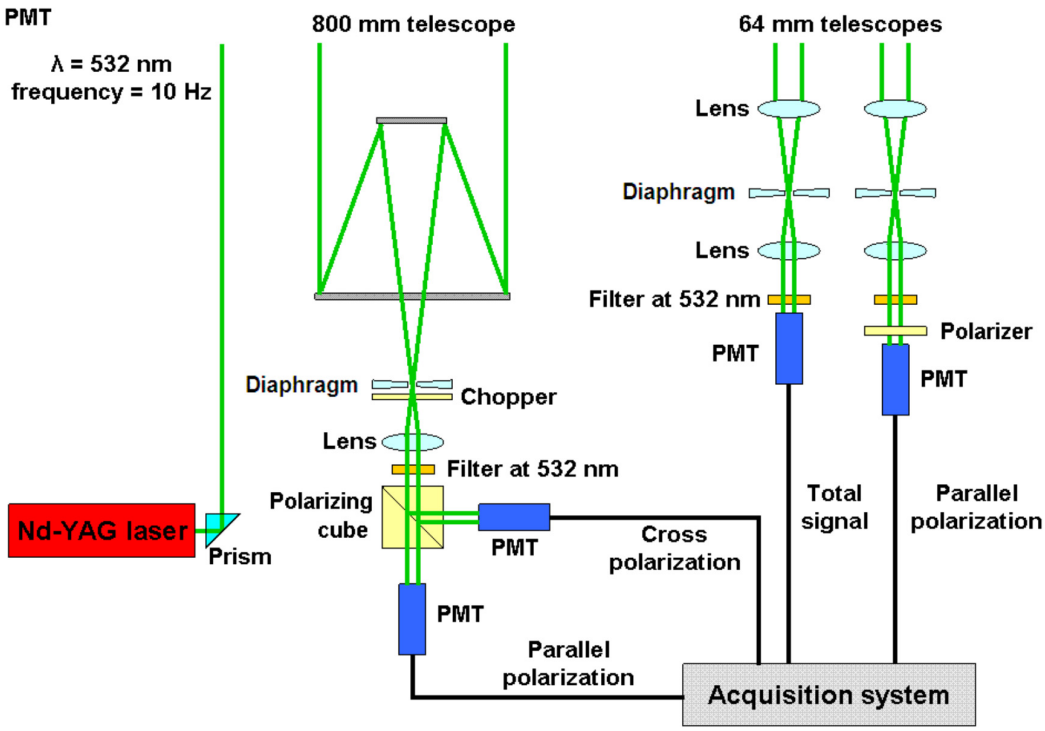

Figure 6. Scheme of the lidar installed at Thule; the receiving system for the upper atmosphere (high altitude channels) is on the left, while the two receivers for the low altitudes are on the right.

N_2O, CO and HNO_3, as well as the H_2O continuum, with a spectral window of 600 MHz tunable between approximately 230 and 280 GHz (or 7.7 and 9.3 cm^{-1}) [e.g., Cheng et al. 1996, de Zafra et al. 1997, Muscari et al. 2007, Fiorucci et al. 2008]. Figure 3 shows the GBMS in its present setup at Thule. It was designed and built at the Physics and Astronomy Department of the State University of New York at Stony Brook and comprises a front end receiver employing a cryogenically cooled SIS (superconductor-insulator-superconductor) double sideband mixer with an intermediate frequency (IF) of 1.4 GHz. The back end is composed of an acousto-optical spectrometer (AOS) with a spectral band pass of 600 MHz and a maximum resolution of 65 kHz. Details of the apparatus and observing method are covered in Parrish et al. [1988] and de Zafra [1995]. A condensed description of the observing method is outlined below. The GBMS observes the emission line of one chemical species at a time, usually for 1 to 5 hours (depending on S/N). Its 600 MHz window is then tuned to a different frequency interval (in the 230-280 GHz range) in order to observe the emission line of another chemical species.

Given the physical parameters of a specific rotational transition, its spectral line shape depends strongly on the vertical concentration profile of the observed species (typically unknown), strongly on the atmospheric pressure profile and less strongly on the temperature profile (both typically known). Therefore, by means of the observed line shape together with pressure and temperature vertical profiles, a mathematical deconvolution process allows finding the emitting molecule's concentration as a function of altitude through various mathematical 'deconvolution' procedures [e.g., Rodgers 2000]. The overall spectral band pass and resolution of the GBMS are key elements to determine the 17-75 km altitude range where trace gases concentration can be measured. For water vapor, we do not observe an H_2O emission line (e.g., at 183 or 325 GHz) but rather the emission from the H_2O continuum existing between emission lines. Therefore, only the integrated column contents can be obtained from GBMS observations of water vapor [Fiorucci et al. 2008].

During normal data-taking operations the GBMS observes radiation from two different directions 75° to 80° apart, switched by a rotating reflective semicircular chopper wheel at ~1 Hz frequency. One observing direction is near the zenith (reference beam, or R) while the other points between 10° and 15° above the horizon (signal beam, or S). A dielectric sheet (made of Plexiglas) mounted in the R beam acts as a local partially transparent (and weakly emitting) 'grey body' source of broadband radiation to compensate for the lower total power received from atmospheric emission near the zenith (with a shorter geometrical path length with respect to the S beam), and allows a power balance to be achieved between the S and R beam directions. Different dielectric sheets are used, depending on atmospheric conditions, with their opacity ranging from ~0.2 to 0.8 Nepers at 275 GHz. This power balance is sensed by a phase-sensitive detector synchronized to the rotation of the beam-

switching chopper wheel, and maintained by a servo system which adjusts the elevation angle of the S beam if the (S-R) power level deviates from zero. As atmospheric opacity increases or decreases (causing thermal emission from the atmosphere to increase or decrease), the servo mechanism, seeking to maintain power balance in the two beams, will drive the S-beam angle upwards or downwards. The opacity of the dielectric sheet, dependent on its composition and thickness, will determine the equilibrium angles for a given range of atmospheric opacity. Atmospheric radiation from both beam directions enters through a window made of type PP-2 Eccofoam characterized by a very small opacity at millimeter wavelengths (~0.007 Nepers). This sensitivity of observing-beam elevation angle to total water vapor opacity allows a continuous measure of integrated water column overhead, while the spectral data (line shape and intensity), deconvolved against measured temperature and pressure profiles, allows retrieval of the mixing ratio of a particular molecular trace gas with altitude. Overall accuracy estimates for various molecular mixing ratio profile retrievals are altitude and species dependent, and are given in Parrish et. al. [1988], de Zafra [1995], and Fiorucci et al. [2011].

2.3. Broadband shortwave and infrared radiometers

Different pyranometers and pyrgeometers for the measurement of the solar and infrared irradiance at the surface have been installed at Thule in different periods starting from 2002. All the radiometers were placed on the roof of building #1985 at South Mountain (Figure 4).

A Yankee Environmental System ventilated Total solar pyranometer (YES TSP-700) was installed by DMI in 2002. The TSP is a WMO (World Meteorological Organization) second class pyranometer and measures shortwave global irradiance in the spectral range 0.3-3.0 μm, I_{SW}. The TSP was calibrated in 1998, and checked once a year after its installation with a reference lamp: the integrated lamp irradiance measured by the TSP in the different years is always within 2% of the lamp nominal emission. The total uncertainty on the shortwave global irradiance measurements is less than 2.5% for a solar zenith angle $\theta \leq 75°$ and less than 3.4% for $75° < \theta \leq 85°$ [Di Biagio et al. 2012]. In the period February-August 2009 also an Eppley precision spectral pyranometer (PSP) was installed at TAB by ENEA to be compared with TSP. A further comparison with another recently calibrated PSP was carried out at Thule during the field campaign 2010-2011. Data indicate that the TSP and PSP radiometers agree within ±3% for $\theta < 70\%$, thus confirming the TSP accuracy of ±2.5%.

Because of the annual evolution of the solar illumination at TAB, the TSP is installed from mid-February to mid-October each year. The minimum of the solar zenith angle is ~52° at the summer solstice.

A ventilated Eppley precision infrared radiometer (PIR) was installed at Thule in February 2009. The PIR is a WMO first class pyrgeometer that measures the downward longwave irradiance in the spectral range 3.5-50 μm, I_{LW}. The downward irradiance is derived from the measured signal and instrument temperatures using the Albrecht and Cox [1977] formula. The PIR calibration was verified by comparison with a recently calibrated PIR installed at the ENEA station at Lampedusa (http://www.lampedusa.enea.it/) in 2008. Additional calibrations were made at Thule by comparison with two CGR4 pyrgeometers during 2010 and 2011. The calibration error is estimated to be less than 1%. The total uncertainty associated with the PIR measurements is less than 1.7%.

The radiometers installed at #1985 have the horizon free from obstacles; the domes of the instruments are cleaned weekly and the data are acquired every minute. An automatic weather station is also operational on the roof of building #1985.

2.4. The Cimel sunphotometer

A Cimel sunphotomer (Figure 5) [Holben et al. 1998] has been operational at Thule since 2007. The Cimel sunphotometer measures direct sun and sky radiances at eight narrowband channels (340, 380, 440, 500, 670, 870, 940, and 1020 nm). Cimel measurements are used to derive the aerosol optical depth and the water vapour column content, as well as other aerosol physical properties. The Cimel is operated at Thule in the period March-October, when the Sun is above the horizon at least during part of the day.

The Cimel (see Figure 5) is composed by a sensor head fixed to a robot base, which in turn is connected to two motors that allow its rotation over the horizontal and the vertical planes; the sensor head is connected to a 33 cm long collimator able to point at the sun or at the sky with a field of view of ±1.2°. The Cimel is provided with eight interference filters centered at the eight used wavelength. The radiation transmitted by each filter is then received by a silicon photodiode which produces a voltage as output. The sequence of measurements in the eight spectral bands requires about 10 seconds; a series of three measurements, for a total of 30 seconds, is taken for each observation.

The instrument measures in direct sun and sky modes. In direct sun mode the instrument points at the sun; these measurements are performed about every 15 minutes and are used to derive, by applying the Beer-Bouguert-Lambert law, the aerosol optical depth and

the water vapour atmospheric content. In sky mode the instrument measures radiation coming from the sky in four spectral bands (440, 670, 870, and 1020 nm). Measurements are taken over the solar principal plane (at constant azimuth angle and varying the scattering angle) up to nine times a day, and along the solar almuncantar (constant elevation angle and varying the azimuthal angle) up to six times a day, both in the morning and in the afternoon. Sky mode measurements are used to derive aerosol optical and microphysical properties, such as size distribution, phase function, single scattering albedo, and asymmetry factor among others, through the application of inversion procedures [Dubovik and King 2000].

3. Field activities and meteorological constraints

During the 2009 IPY field campaign, most of the Italian instrumentation was set up in the main base, at building #216, which is a 10-minute walk from the NSF living quarters and even closer to the dining hall. Regularly, about once every 3 or 4 days, a trip to South Mountain was necessary in order to control the correct operation of the radiometers installed on the roof of building #1985. This required a 20-minute drive (each way) to South Mountain by means of a car provided by the DMI.

Lidar and GBMS data taking campaigns occur mainly in winter, when the stratospheric processes that generate ozone depletion take place and when the observing conditions are favourable. The Arctic middle stratospheric vortex forms in winter and vanishes in early spring, and it is inside this large vortex that GBMS and lidar observing efforts of stratospheric parameters have been concentrated. At the same time, the GBMS needs a low content of water vapor in the troposphere in order to measure the emission of stratospheric chemical constituents with sufficient accuracy, and this condition is realized only during winter months. Furthermore, lidar observations of the middle atmosphere are best carried out during darkness, as sunlight is a relevant source of noise. All these elements force the field team to operate at Thule during winter, when meteorological conditions are severe but long stretches of nighttime are available. Two or more intense snow storms are expected during each winter field campaign, with winds gusts that may reach 200 km/h and the windchill plunging to –60°C. Storms usually imply 3-4 days in which no travel outside or even inside the base is permitted and no instrumentation can be operated. During the field campaign of 2008-2009, a long stretch of bad weather with short-lived storms hit from February 5 to 11.

Figure 7 shows the 1951 to 2006 monthly mean of surface temperatures, winds, and precipitation over

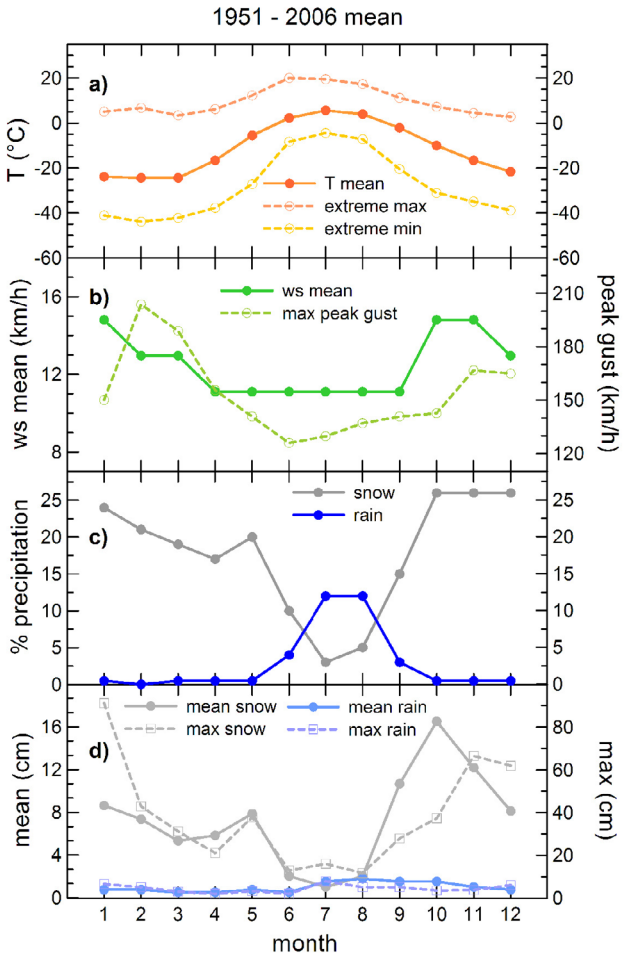

Figure 7. 1951 to 2006 monthly mean of: (a) surface temperature, T, and its maximum and minimum extremes; (b) surface wind speed (ws) and maximum gust speed; (c) fractional amount (in percent) of precipitations as rain and snow; (d) mean and maximum rainfall and snowfall.

Thule. In winter ground temperatures regularly reach –25°C; extreme minima of –45°C were measured during very cold years. The maximum probability of snow precipitations, ~20-25%, is in winter, with a mean of 15 cm of snow and a maximum of 60-90 cm between November and January.

4. Studies on the lower and upper atmosphere

4.1. Troposphere observations

Figure 8 shows the daily mean meteorological parameters measured at Thule in the period 2007-2009. Daily surface temperatures vary between a winter minimum of about –33°C to a summer maximum of about +7°C. The variability is the strongest in winter. The daily mean T is above 0°C in June, July, and August, and below –20°C from November to April. The surface pressure also shows an annual cycle, with larger values in summer, up to about 1000 hPa, and lower values, down to about 960 hPa, in winter. The daily mean wind speed (WS) reaches peak values of 25 m/s, while it is < 5 m/s

in the majority of cases. The observed T and WS during 2007-2009 are in agreement with the long-term mean values reported in Figure 7, thus indicating no extreme cold or warm conditions in the three considered years. The wind direction (WD) shows a clear annual evolution, with WD<150° during winter, with frequent katabatic winds from the ice cap, and WD>150°, from the sea surface, throughout the rest of the year. The daily mean measured relative humidity over water (RH_W) and the derived RH over ice (RH_I) are also shown in Figure 8. RH_I is between 60 and 95% in the period November to April, when T<–20°C, and lower in the remaining part of the year; T~–15°C was indicated by Curry et al. [1990] as the threshold temperature for the onset of the ice nucleation in the Arctic. RH_W varies between 35 and 75% and shows a small annual cycle, with larger values in summer and lower in winter.

The all-sky daily mean shortwave (I_{SW}) and longwave (I_{LW}) irradiances are shown in Figure 9. I_{SW} shows a strong annual cycle, due to the annual evolution of the solar zenith angle, with values close to zero in February and October and peaks in the summer months. The maximum of about 360 Wm^{-2} is observed in June, when the solar zenith angle reaches its minimum of ~52° and 24 hours of daylight are present. The daily I_{SW} strong variability is primarily due to clouds, which may produce a reduction of the daily I_{SW} as large as 85%.

The clear-sky shortwave radiation at the surface is mainly affected by water vapour absorption, which produces a reduction of I_{SW} as large as 65 Wm^{-2} (12%) during summer. The seasonal change of the albedo produces an increase of I_{SW} by up to 25 Wm^{-2} (4.5%) in spring. The annual mean radiative effect is estimated to be –(10÷11) Wm^{-2} for water vapour and +(2÷3) Wm^{-2} for the albedo. Aerosols also contribute, in smaller amounts, to the surface radiation budget [Di Biagio et al. 2012].

Surface conditions vary largely during the year, and snow and sea-ice coverage show a defined seasonal cycle. Measurements performed by the spectroradiometer MODIS [Xiong and Barnes 2005] on board Terra and Aqua satellites are used to derive the 8-day surface shortwave albedo over Thule (Figure 10, center panel). The surface albedo varies between 0.05 and 0.66, showing a strong annual cycle. The shortwave albedo is larger than 0.5 in spring, when the surface is covered by snow/ice, with a maximum between March and April. In summer, with the melting of surface snow and sea-ice, the albedo drops to values of about 0.05-0.1. The transition from high to low albedo occurs at Thule typically between mid-May and mid-June, in correspondence with the increase of the temperatures above freezing, and lasts for about three weeks.

Figure 10 (upper and lower panels) shows the

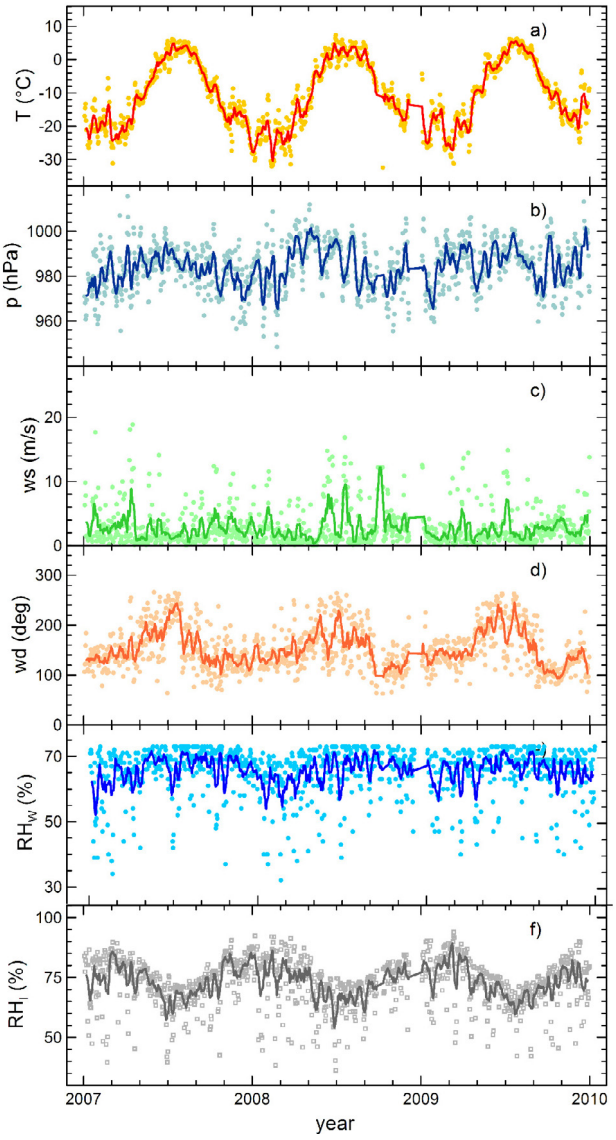

Figure 8. Daily means of: (a) air temperature, T; (b) surface pressure, p; (c) wind speed, ws; (d) wind direction, wd; (e, f) relative humidity with respect to water, RH_W, and ice, RH_I, measured at Thule in the period 2007-2009. 10-day running means (solid lines) are also shown.

aerosol optical depth (AOD) at 500 nm and the column water vapour derived at Thule by means of Cimel observations. The column integrated water vapour (wv) varies between 0.1 and 1.4 cm showing a well defined annual cycle with values lower than 0.6 cm in spring and early-autumn, and up to 1.4 cm, in summer. The water vapour peak occurs in July and the absolute maximum, 1.62 cm, was measured on July 17, 2009. The uncertainty on the retrieved wv is <12%.

The aerosol optical depth is generally lower than 0.2 and shows a defined annual cycle, with larger values during spring, in correspondence with the haze season [Quinn et al. 2007]. The lowest values of AOD are observed in summer, when pristine marine background conditions typically occur and the advection of air masses carrying aerosol originated at low latitudes is strongly suppressed. Isolated events of long range transport,

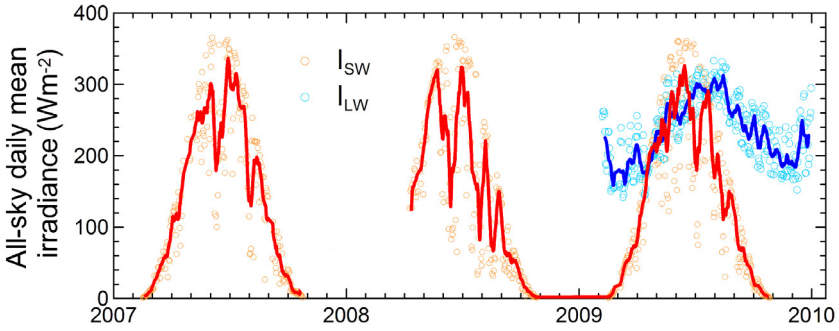

Figure 9. All-sky daily mean shortwave and longwave irradiance measured at Thule between 2007 and 2009 with the TSP-700 and the PIR 33499. The 10-day running mean (solid lines) is also shown.

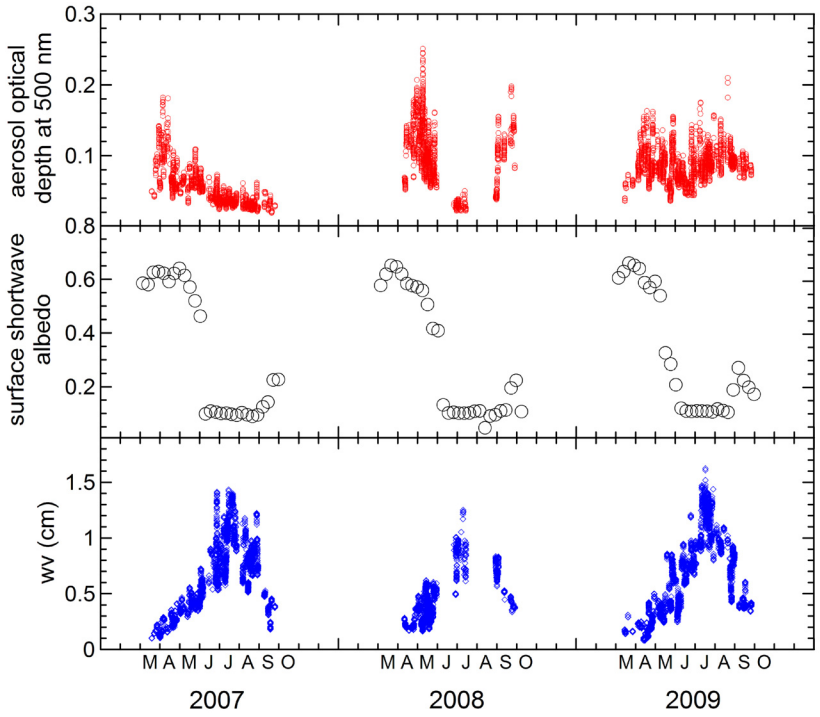

Figure 10. Top panel: aerosol optical depth at 500 nm. Bottom panel: column water vapour (wv) derived from Cimel observations. Center panel: MODIS derived 8-day surface shortwave albedo during the period March-October of the years 2007-2009.

mainly from Eurasia, may determine local large increases in optical depth. For instance, the absolute maximum of optical depth, ~0.25, observed at Thule on May 8, 2008, was related to an event of biomass burning occurred in central Russia, which largely affected the whole Arctic area in the period April-May of that year [e.g., Warneke et al. 2009]. Another example is the relative large values of optical depth observed in summer 2008 and 2009 (AOD > 0.1), which can be associated to episodes of transport of polluted particles from central and western Europe. AOD observations at Thule are in good agreement with data reported at several other Arctic sites in recent years [e.g., Tomasi et al. 2007 and 2012, Stone et al. 2010, Rodríguez et al. 2012].

The PIR was installed at Thule in 2009, and only one year of measurements of I_{LW} is available. The daily I_{LW} varies from ~130 Wm^{-2} in winter to ~350 Wm^{-2} in summer, with the maximum observed between July and August; the annual cycle of I_{LW} primarily follows that of surface temperature and, to a minor extent, that of water vapour. Clouds play a large role in affecting the magnitude of the longwave radiation at the surface; while atmospheric aerosols contribute in minor part. The effect of clouds is largest in winter, with an increase in I_{LW} by up to 100 Wm^{-2} during cloudy days, and somewhat smaller in summer.

As it is evident from Figure 9 and also from Figure 11 where the ratio between I_{SW} and I_{LW} is shown for 2009, the longwave radiation plays a large role throughout the year, and is the dominant component in all seasons except summer. Even in summer, the daily average LW component exceeds the SW component when thick clouds are present. The occurrence of clouds, generally leading to a reduction of I_{SW} and an enhancement of I_{LW}, tends to increase the role of longwave radiation on the radiation budget.

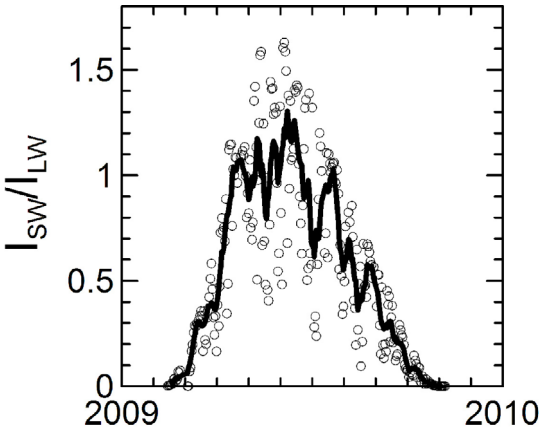

Figure 11. Ratio of the shortwave to longwave irradiance measured at Thule in 2009.

4.2. Stratospheric observations during the IPY

The first part of winter 2008-2009 has been characterized by a stable and cold polar vortex which allowed the persistent formation of PSC particles. In mid-January of 2009, however, the most intense sudden stratospheric warming (SSW) ever observed occurred [Manney et al. 2009, Di Biagio et al. 2010]. SSWs strongly affect the dynamics and thermal structure of the Arctic stratosphere causing the breakdown of the eastward winter circulation, the build up of a westward circulation, and the reversal of the latitudinal temperature gradient. As the 2009 SSW developed, the stratopause lowered, the mean zonal circulation reversed, and ultimately the polar vortex in the lower stratosphere split in two (see Figure 12).

Figure 13 shows the lidar backscatter ratio (both parallel and cross polarized components) and the depolarization ratio on January 17 and 18, when the lidar detected a PSC layer. The layer extended between 16 and 23 km altitude on January 17 and then it moved to slightly lower altitudes (16-20 km) on January 18. The observed PSCs can be classified as type Ia due to their low backscatter ratio and moderate depolarization values [e.g., Browell et al. 1990, Toon et al. 1990]. This indicates that their particles are liquid and composed of nitric acid trihydrate (NAT), as also suggested by the temperature values at the altitudes of the observed PSC layer (not shown) which are below the NAT threshold.

Lidar and GBMS measurements at Thule observed the occurrence of the major SSW, sampling air inside the polar vortex at first and following the propagation of the SSW down to the lower stratosphere afterwards. The contour plots in Figures 14, 15, and 16 show the changes of the atmospheric chemical composition over Thule and temperature associated with the SSW. Figure 14 shows a sudden increase in N_2O mixing ratio (mr) which occurred on January 24 at around 35 km altitude and over the whole stratosphere between days 26 and 28. At higher levels, the vortex splitting and the vortex edge transit over Thule was marked by a rapid decrease in CO mr. CO data (not shown) indicate that in the upper stratosphere (45-50 km) the vortex broke up over Thule on January 19-20.

Concurrently, as warm, O_3-rich air from outside the vortex moved over Thule during the SSW, the GBMS measured an increase in O_3 mr in the upper stratosphere which reached a peak of ~8 ppmv at 35 km (Figure 15). The O_3 concentration in the lower stratosphere shows a clear sign of the passage of the vortex edge

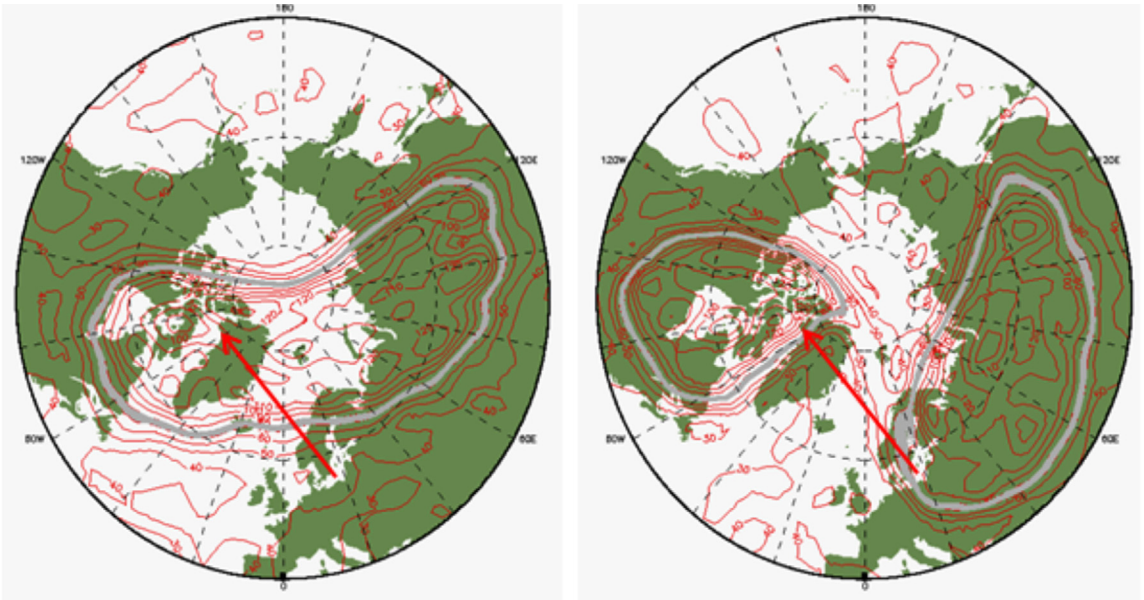

Figure 12. Potential vorticity (PV) contour maps at 550 K (22-23 km altitude) from ECMWF reanalyses showing the splitting of the Arctic polar vortex occurring (at this altitude) between January 23 (map on the left) and 27 (map on the right). The red arrows point to the northwestern coast of Greenland where Thule is located.

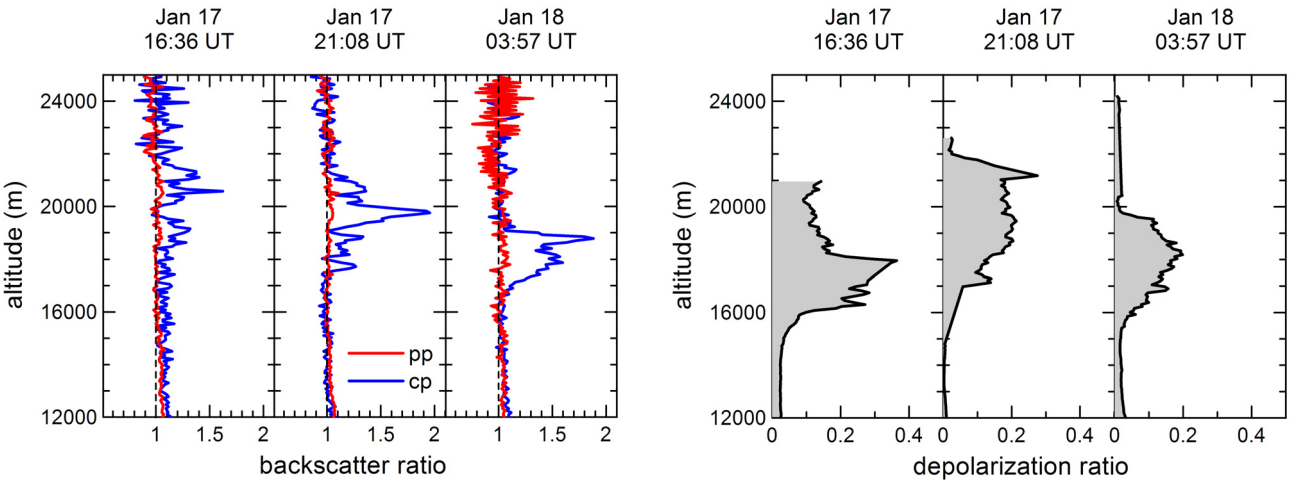

Figure 13. Lidar derived backscatter (left panel) and depolaritazion (right panel) ratioes between 12 and 25 km for the parallel and cross polarized components of the signal acquired on January 17 at 16:36 UT and 21:08 UT , and on January 18 at 03:57 UT.

over Thule on January 26, in agreement with the N_2O concentration displayed in Figure 14, but there are signs of out-vortex air intrusions also a few days earlier. In Figure 16 lidar temperatures show a sudden increase on late January 22. However, the warming in the upper stratosphere started a few days earlier, as shown by the superimposed Aura MLS temperatures, and lidar measurements missed the onset of the SSW due to instrumental upgrades between January 16 and 22. The maximum physical temperature of 289 K was recorded by lidar near 40 km on January 22. In the following days, the warming progressed downward reaching about 15 km altitude on January 29, when the temperature profile became nearly isothermal, particularly in the altitude layer between 15 and 45 km.

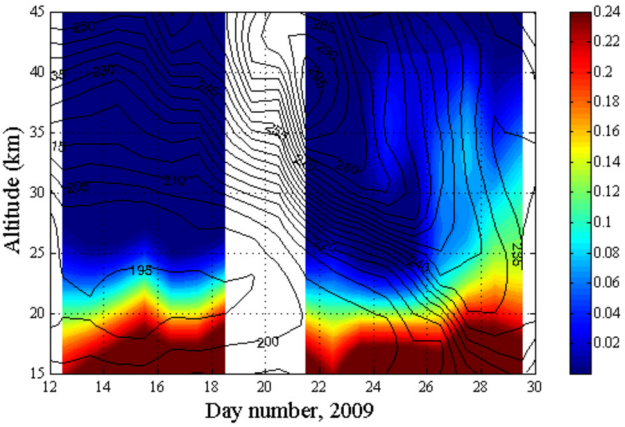

Figure 14. Contour map of GBMS N_2O vmr (in color, units of ppmv). Solid black contour lines depict temperature measurements obtained with the satellite-based Aura MLS instrument.

5. What happened after the IPY and future developments

Starting in October 2010, all the atmospheric remote sensing equipment located on base at building #216 was moved to South Mountain, in a renovated large building #1971 (see Figure 17). The 2010-2011 field campaign at the new location started in late January and ended in early March 2011 and was very suc-

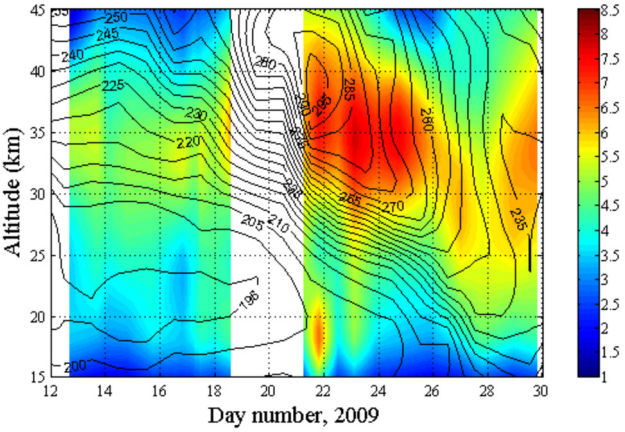

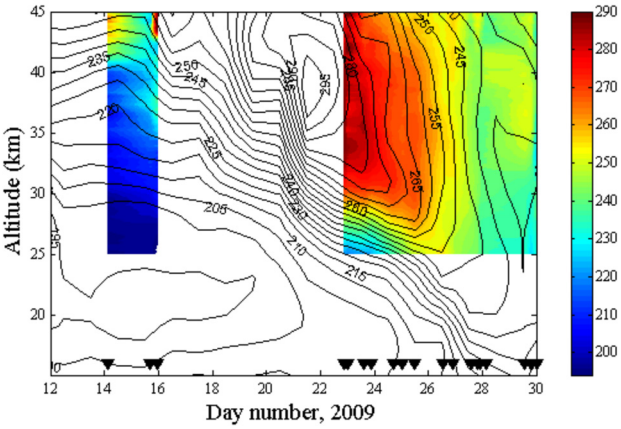

Figure 15 (left panel). Contour map of GBMS O_3 vmr (in color, units of ppmv). Solid black contour lines depict temperature measurements obtained with the satellite-based Aura MLS instrument. **Figure 16** (right panel). Contour map of temperature values (in units of K) obtained from lidar measurements (in color). Solid black contour lines depict temperature measurements obtained with the satellite-based Aura MLS instrument. Solid black triangles at the base of the plot show when lidar measurements were carried out.

Figure 17. Building #1971 (left) and the DMI balloon house at its new location on South Mountain, next to building #1971 (right).

cessful. The move also involved the DMI equipment, including the balloon house used for preparing and launching the ozonesondes, which was previously located near the airport. Together with the relocation of additional remote sensing equipments already present on South Mountain at building #1985, such as the NCAR FTIR, the DMI UV spectrometer, and the ENEA radiometers, which occurred in summer 2011, this major move created a large, international, and multi-instrumental atmospheric remote sensing laboratory at Thule Air Base. The renovated building was modified to host both the GBMS and the lidar, with their specific requirements of electric power, windows and a roof hatch. The altitude of the site (225 m above sea level) and its distance to the main base has both positive and negative points. The GBMS can count on a decrease in atmospheric opacity, albeit small, whereas the lidar loses the possibility of observing the bottom layers of the boundary layer. On the logistics front, the new setup involves the daily use of a car to go back and forth from the main base to building #1971, which is a drawback, but offers the advantages of having all the equipments in one laboratory, supervised in principle by a single unit of personnel.

During the winter campaign of 2011-2012, the lidar system will be upgraded with a more powerful laser source that will allow the lidar temperature measurements to reach higher altitudes and improve on their time resolution. The new laser will have the capabilities of being remotely controlled, which will be useful for operating it from main base or even from Italy, when necessary. This improvement will include mounting small motors that can adjust the direction of the laser beam and of the small telescopes to make it possible to align all the lidar receiving channels by remote control. In the future, lidar operations could be performed at Thule by local personnel that simply turn on and off the electronics and by specialized personnel at the University of Rome that can act on data taking runs and adjust the alignment of the system when necessary. As a part of this collaboration, in the near future we also plan on installing at Thule a new 22 GHz spectrometer for the observation of water vapor stratospheric vertical profiles, at the moment under development at the INGV. This effort is aimed at long term measuring of one of the most important parameters of the middle atmosphere, a key element for detecting the first effects of climate change on the middle atmosphere and on the ozone depletion.

Acknowledgements. This material is based on work also supported by the National Science Foundation under grant 0936365 and by the Programma Nazionale di Ricerca in Antartide (PNRA) under grant 2009/A3.04. We would like to thank David Seibert of the Thule Air Base Weather Forecast Office for providing the 1951-2006 meteorological data, the ECMWF for its temperature and pressure reanalyses, and the MLS team at JPL for the Aura MLS temperature data. MODIS data are distributed by the Land Processes Distributed Active Archive Center (LP DAAC), located at the US Geological Survey (USGS) Earth Resources Observation and Science (EROS) Center (lpdaac.usgs.gov). Very sadly, Prof. Giorgio Fiocco passed away in July 2012. The Italian atmospheric remote sensing activities at Thule, which started back in 1990, the international collaborations and all the science that originated from these 20+ years at Thule have his signature, his crucial and enlightening contribution.

References

Albrecht, B., and S.K. Cox (1977). Procedures for improving pyrgeometer performance, J. Appl. Meteor., 16, 188-197.

Browell, E.V., C.F. Butler, S. Ismail, P.A. Robinette, A.F. Carter, N.S. Higdon, O.B. Toon, M.R. Schoeberl and A.F. Tuck (1990). Airborne lidar observations in the wintertime Arctic stratosphere: Polar stratospheric clouds, Geophys. Res. Lett., 17, 385-388.

Cheng, D., R.L. de Zafra and C. Trimble (1996). Millimeter wave spectroscopic measurements over the South Pole, 2. An 11-month cycle of stratospheric ozone observations during 1993-1994, J. Geophys. Res., 101, 6781-6793.

Curry, J.A., F.G. Meyer, L.F. Radke, C.A. Brock and E.E.

Ebert (1990). Occurrence and characteristics of lower tropospheric ice crystal in the Arctic, Int. J. Climatol., 10, 749-764.

de Zafra, R.L. (1995). The ground-based measurements of stratospheric trace gases using quantitative millimeter wave emission spectroscopy, In: G. Fiocco and G. Visconti (eds.), Diagnostic tools in atmospheric physics, Proceedings of the International School of Physics "Enrico Fermi", Società Italiana di Fisica, Bologna, 23-54.

de Zafra, R.L., V. Chan, S. Crewell, C. Trimble and J.M. Reeves (1997). Millimeter wave spectroscopic measurements over the South Pole: 3. The behavior of stratospheric nitric acid through polar fall, winter, and spring, J. Geophys. Res., 102 (D1), 1399-1410.

Di Biagio, C., G. Muscari, A. di Sarra, R.L. de Zafra, P. Eriksen, I. Fiorucci and D. Fuà (2010). Evolution of temperature, O_3, CO, and N_2O profiles during the exceptional 2009 Arctic major stratospheric warming as observed by lidar and mm-wave spectroscopy at Thule (76.5°N, 68.8°W), Greenland, J. Geophys.Res., 115, D24315; doi:10.1029/2010JD014070.

Di Biagio, C., A. di Sarra, P. Eriksen, S.E. Ascanius, G. Muscari and B. Holben (2012). Effect of surface albedo, water vapour, and atmospheric aerosols on the cloud-free shortwave radiative balance in the Arctic, Clim. Dyn., 39 (3), 953-969; doi:10.1007/s00382-011-1280-1.

Di Girolamo, P., M. Cacciani, A. di Sarra, G. Fiocco and D. Fuà (1994). Lidar observations of the Pinatubo aerosol layer at Thule, Greenland, Geophys. Res. Lett., 21, 1295-1298 doi:10.1029/93GL02892.

di Sarra, A., M. Cacciani, P. Di Girolamo, G. Fiocco, D. Fuà, B. Knudsen, N. Larsen and T.S. Jørgensen (1992). Observations of correlated behavior of stratospheric ozone and aerosol at Thule during winter 1991-92, Geophys. Res. Lett., 19, 1823-1826.

di Sarra, A., M. Cacciani, G. Fiocco, D. Fuà, T.S. Jørgensen, B. Knudsen, N. Larsen and I.B. Mikkelsen (1995). Ozone and aerosol correlated observations at Thule, Greenland, in the period 1991-1994, J. Geophys. Res., 100, 25965-25977; doi:10.1029/95JD02906.

di Sarra, A., L. Bernardini, M. Cacciani, G. Fiocco and D. Fuà (1998). Stratospheric aerosols observed by lidar over northern Greenland in the aftermath of the Pinatubo eruption, J. Geophys. Res., 103, 13873-13891.

di Sarra, A., M. Cacciani, G. Fiocco, D. Fuà and T.S. Jørgensen (2002). Lidar observations of polar stratospheric clouds over northern Greenland in the period 1990-1997, J. Geophys. Res., 107 (D12); doi:10.1029/2001JD001074.

Dubovik, O., and M.D. King (2000). A flexible inversion algorithm for retrieval of aerosol optical properties from Sun and sky radiance measurements, J. Geophys. Res., 105, 20673-20696.

Fiorucci, I., G. Muscari, C. Bianchi, P. Di Girolamo, F. Esposito, G. Grieco, D. Summa, G. Bianchini, L. Palchetti, M. Cacciani, T. Di Iorio, G. Pavese, D. Cimini and R.L. de Zafra (2008). Measurements of low amounts of precipitable water vapor by millimeter wave spectroscopy: An intercomparison with radiosonde, Raman lidar, and Fourier transform infrared data, J. Geophys. Res., 113, D14314; doi:10.1029/2008JD009831.

Fiorucci, I., G. Muscari and R.L. de Zafra (2011). Revising the retrieval technique of a long-term stratospheric HNO_3 data set: from a constrained matrix inversion to the optimal estimation algorithm, Annales Geophysicae, 29, 1317-1330; doi:10.5194/angeo-29-1317-2011.

Holben, B.N., T.F. Eck, I. Slutsker, D. Tanre, J.P. Buis, A. Setzer, E. Vermote, J.A. Reagan, Y. Kaufman, T. Nakajima, F. Lavenu, I. Jankowiak and A. Smirnov (1998). AERONET - A federated instrument network and data archive for aerosol characterization, Rem. Sens. Environ., 66, 1-16.

Larsen, N., B. Knudsen, T.S. Jørgensen, A. di Sarra, D. Fuà, P. Di Girolamo, G. Fiocco, M. Cacciani, J.M. Rosen and N.T. Kjome (1994). Backscatter measurements of stratospheric aerosols at Thule during January-February 1992, Geophys. Res. Lett., 21, 1303-1306.

Manney, G.L., M.J. Schwartz, K. Kruger, M.L. Santee, S. Pawson, J.N. Lee, W.H. Daffer, R.A. Fuller and N.J. Livesey (2009). Aura Microwave Limb Sounder observations of dynamics and transport during the record-breaking 2009 Arctic stratospheric major warming, Geophys. Res. Lett., 36, L12815; doi:10.1029/2009GL038586.

Marenco, F., A. di Sarra, M. Cacciani, G. Fiocco and D. Fuà (1997). Thermal structure of the winter middle atmosphere observed by lidar at Thule, Greenland, during 1993-94, J. Atmos. Sol.-Terr. Phys., 59, 151-158; doi:10.1016/1364-6826(95)00198-0.

McGuire, A.D., F.S. Chapin III, J.E. Walsh and C. Wirth (2006). Integrated regional changes in Arctic climate feedbacks: Implications for the global climate system, Annu. Rev. Environ. Resour., 31, 61-91.

Muscari, G., A.G. di Sarra, R.L. de Zafra, F. Lucci, F. Baordo, F. Angelini and G. Fiocco (2007). Middle atmospheric O_3, CO, N_2O, HNO_3, and temperature profiles during the warm Arctic winter 2001-2002, J. Geophys. Res., 112, D14304; doi:10.1029/2006JD007849.

Parrish, A., R.L. de Zafra, P.M. Solomon and J. W. Barrett (1988). A ground-based technique for millimeter

wave spectroscopic observations of stratospheric trace constituents, Radio Sci., *23*, 106-118.

Quinn, P., G. Shaw, E. Andrews, E. Dutton, T. Ruoho-Airola and S. Gong (2007). Arctic haze: Current trends and knowledge gaps, Tellus B, *59*, 99-114.

Rodgers, C.D. (2000). Inverse method for atmospheric sounding, Series on Atmospheric, Oceanic and Planetary Physics - vol. 2, Taylor, F.W., World Scientific Publishing Co. Pte LTd, Singapore.

Rodríguez, E., C. Toledano, V. Cachorro, G. de Leeuw, A. De Frutos, M. Gausa and B. Holben (2012). Comparison of aerosol optical properties at the sub-arctic stations ALOMAR-Andenes, Abisko and Sodankylä in late spring and summer 2007, Atmos. Res., 107, 20-30.

Serreze, M.C., and J.A. Francis (2006). The Arctic amplification debate, Clim. Change, 76, 241-264.

Stone, R.S., A. Herber, V. Vitale, M. Mazzola, A. Lupi, R.C. Schnell, E.G. Dutton, P.S. K. Liu, S.-M. Li, K. Dethloff, A. Lampert, C. Ritter, M. Stock, R. Neuber and M. Maturilli (2010). A three-dimensional characterization of Arctic aerosols from airborne Sun photometer observations: PAM-ARCMIP, April 2009, J. Geophys. Res., 115, D13203; doi:10.1029/2009JD013605.

Tomasi, C., V. Vitale, A. Lupi, C. Di Carmine, M. Campanelli, A. Herber, R. Treffeisen, R.S. Stone, E. Andrews, S. Sharma, V. Radionov, W. von Hoyningen-Huene, K. Stebel, G.H. Hansen, C.L. Myhre, C. Wehrli, V. Aaltonen, H. Lihavainen, A. Virkkula, R. Hillamo, J. Ström, C. Toledano, V. E. Cachorro, P. Ortiz, A.M. de Frutos, S. Blindheim, M. Frioud, M. Gausa, T. Zielinski, T. Petelski and T. Yamanouchi (2007). Aerosols in polar regions: A historical overview based on optical depth and *in situ* observations, J. Geophys. Res., 112, D16205; doi:10.1029/2007JD008432.

Tomasi, C., A. Lupi, M. Mazzola, R. Stone, E. Dutton, A. Herber, V. Radionov, B. Holben, M. Sorokin, S. Sakerin, S. Terpugova, P. Sobolewski, C. Lanconelli, B. Petkov, M. Busetto and V. Vitale (2012). An update on polar aerosol optical properties using POLAR-AOD and other measurements performed during the International Polar Year, Atmos. Environ., 52, 29-47.

Toon, O.B., E.V. Browell, S. Kinne and J. Jordan (1990). An analysis of lidar observations of polar stratospheric clouds, Geophys. Res. Lett., 17, 393-396.

Warneke, C., R. Bahreini, J. Brioude, C.A. Brock, J.A. de Gouw, D.W. Fahey, K.D. Froyd, J.S. Holloway, A. Middlebrook, L. Miller, S. Montzka, D.M. Murphy, J. Peischl, T.B. Ryerson, J.P. Schwarz, J.R. Spackman and P. Veres (2009). Biomass burning in Siberia and Kazakhstan as an important source for haze over the Alaskan Arctic in April 2008, Geophys. Res. Lett., 36, L02813; doi:10.1029/2008GL036194.

Xiong, X., and W. Barnes (2005). MODIS calibration and characterization, In: J. Qu, W. Gao, M. Kafatos, R. Murphy and V. Salomonson (eds.), Earth Science Satellite Remote Sensing, vol. I, ch. 4, Springer-Verlag.

*Corresponding author:Giovanni Muscari,
Istituto Nazionale di Geofisica e Vulcanologia, Sezione Roma 2, Rome, Italy; email: giovanni.muscari@ingv.it.